

Intermolecular Packing in *B. mori* Silk Fibroin: Multinuclear NMR Study of the Model Peptide (Ala-Gly)₁₅ Defines a Heterogeneous Antiparallel Antipolar Mode of Assembly in the Silk II Form

Tetsuo Asakura,^{*,†,‡} Takuya Ohata,[†] Shunsuke Kametani,[§] Keiko Okushita,[†] Koji Yazawa,^{||} Yusuke Nishiyama,^{||} Katsuyuki Nishimura,[‡] Akihiro Aoki,[†] Furitsu Suzuki,[⊥] Hironori Kaji,[⊥] Anne S. Ulrich,[#] and Mike P. Williamson[%]

[†]Department of Biotechnology, Tokyo University of Agriculture and Technology, Koganei, Tokyo 184-8588, Japan

[‡]Institute for Molecular Science, 38 Nishigo-Naka, Myodaiji, Okazaki 444-8585, Japan

[§]Mitsui Chemical Analysis & Consulting Service, Inc., 580-32, Nagaura, Sodegaura, Chiba 299-0265, Japan

^{||}JEOL RESONANCE Inc., 3-1-2 Musashino, Akishima, Tokyo 196-8558, Japan

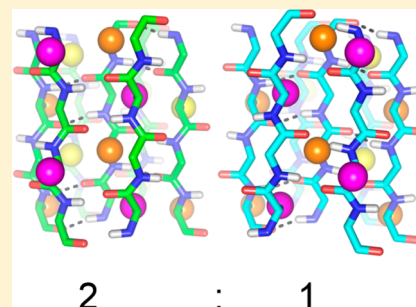
[⊥]Institute for Chemical Research, Kyoto University, Uji, Kyoto 611-0011, Japan

[#]Karlsruhe Institute of Technology, IBG-2 and IOC, Fritz-Haber-Weg 6, 76131 Karlsruhe, Germany

[%]Department of Molecular Biology and Biotechnology, University of Sheffield, Firth Court, Western Bank, Sheffield S10 2TN, U.K.

S Supporting Information

ABSTRACT: We have previously suggested that crystalline *Bombyx mori* silk in silk II form (the silk structure after spinning) is not a simple antiparallel β -sheet but is intrinsically heterogeneous. Using the peptide (AG)₁₅, we have obtained the first fully assigned high resolution solid state ¹H NMR spectrum. Distinct heterogeneity was observed, in both ¹H and ¹³C CP/MAS signals. Based on these results, a new model is proposed that contains two different packing arrangements of antiparallel β -sheets. The structures were energetically minimized by CASTEP calculation and used to calculate the solid state ¹H, ¹³C, and ¹⁵N NMR chemical shifts using the GIPAW method. This new model was supported by good agreement between the calculated and observed ¹H, ¹³C, and ¹⁵N chemical shifts and relative ¹H–¹H proximities obtained from 2D ¹H DQMAS experiments. We conclude that the intermolecular packing of *B. mori* silk fibroin has been finally resolved.



INTRODUCTION

Because of the exceptional strength and toughness of the *Bombyx mori* (silkworm) silk fiber, and in view of increasing applications in the area of biomaterials, much attention has been paid to the structure of silk fibroin.^{1–6} Two crystalline forms, Silk I and Silk II, have been reported as dimorphs, essentially representing the regular domains of fibroin before and after spinning. By using several solid state NMR techniques, the Silk I form (as stored in the *B. mori* silkworm and dried under mild conditions) has been shown to possess a repeated type II β -turn structure.^{7–9} On the other hand, the precise intermolecular packing in the Silk II form (representing the core of the spun silk fiber) has not yet been determined. Using X-ray fiber diffraction of the crystalline region, the structure of Silk II was first characterized by Marsh, Corey, and Pauling¹⁰ as a regular array of antiparallel β -sheets: this structure remains the classic image of β -sheet silk. We call this model the “Marsh model”. Later, Fraser et al.,¹¹ Lotz and Keith,¹² and Fossey et al.¹³ supported the general features of this antiparallel β -sheet model, but some of them also noted an irregular structure to be present in the silk fibers.^{11,12} Takahashi

et al.¹⁴ proposed that a crystal site is statistically occupied by either of two antiparallel β -sheet chains with different relative orientations, in a 2:1 ratio, based on X-ray diffraction analysis of silk fibers. The latter analysis is more detailed and based on better data than the “Marsh model”. We call the model by Takahashi et al. the “Takahashi model”. There are no further reports about *B. mori* silk fiber in Silk II form at atomic level since Takahashi’s paper.

The Takahashi model is a better fit to the experimental data than the Marsh model but is not consistent with the distances of the intermolecular hydrogen bonds between the NH...OC groups of Ala and Gly, as explained below. It is therefore high time to come up with a new comprehensive model for the silk fiber that can satisfy all of the currently contradictory analytical data.

In the present work, a precise model for the crystalline structure of *B. mori* silk fibroin in the Silk II form is presented

Received: October 28, 2014

Revised: December 9, 2014

Published: December 24, 2014

using a small (Ala-Gly)₁₅ peptide as the model. The alternating copolypeptide (Ala-Gly)_n has been generally accepted as a good model of the crystalline region, NMR spectra of (AG)_n correspond closely to those obtained using the crystalline fraction of native silk II fibers,^{7–16} and the torsion angles of the straight backbone chains correspond to the typical angles of an antiparallel β -sheet.¹⁷ In previous ¹³C solid state NMR studies of (AG)_n, the ¹³C β signal of the Ala residues has been reported to consist of three peaks.^{15,16} The high-field peak was assigned to a distorted β -turn/random coil, while the other two peaks were assigned to antiparallel β -sheet structures with different intermolecular arrangements.

¹H NMR spectra are expected to be most sensitive and highly informative about the interstrand packing interactions because ¹H nuclei are located on the surface of macromolecules. Indeed, two-dimensional ¹H DQMAS experiments have been applied to a wide variety of solid systems to determine the relative ¹H–¹H proximities between molecules.^{18,19} Recently, we have developed a 1 mm microcoil MAS NMR probe head for mass-limited solid samples.²⁰ By combining the use of this microcoil probe head with ultrahigh field NMR at 920 MHz, we were able to obtain solid state ¹H NMR spectra with excellent resolution for the (AG)₁₅ model peptide in the Silk I form as well as for several other related peptides.^{9,21,22} Based on these advances, solid state ¹H NMR can now be used to study the intermolecular arrangement of Silk II.

The key challenge lies in the ability to discern and resolve the two kinds of antiparallel β -sheet chains with different intermolecular packing arrangements, as detected here and in the earlier ¹³C CP/MAS NMR study.^{15,16} We therefore carried out a search of packing arrangements, guided by crystallographic and NMR data; refined the resulting structures; and tested them against experimental data. The peptide (AG)_n crystallizes in space group *P*2₁, a rectangular unit cell with the parameters *a* = 9.38 Å, *b* = 9.49 Å, and *c* = 6.98 Å. The Marsh model places the molecular axis along *b* but is otherwise very similar: *a* = 9.40 Å, *b* = 6.97 Å, and *c* = 9.20 Å. In order to generate two kinds of β -sheet models with different intermolecular arrangements, we had the idea to calculate atomic coordinates for the chains, setting either *c* or *b* along the molecular axis. For each of these two models, energy optimization was performed.⁹ ¹H, ¹³C, and ¹⁵N chemical shifts were then predicted for the two antiparallel β -sheet structures using the GIPAW method.²³ Such GIPAW calculations have been widely applied to organic molecules, and their validity has been demonstrated by experimental solid state NMR analyses.^{19,24–34} The ¹³C and ¹⁵N chemical shifts of Silk II are known from previous work and can thus be used to compare and validate the two different structural models based on their predicted chemical shift values.^{35,36} The solid state ¹H NMR chemical shift is particularly sensitive to the intermolecular packing arrangement of Silk II and could thus be used as a reliable tool to judge the validity of any previously proposed models and to propose a new intermolecular arrangement from this study.

EXPERIMENTAL SECTION

Different Isotope-Labeled Peptides (AG)₁₅. Isotope-labeled amino acids ([2-d₁]Ala, [3-¹³C]Ala, [U-¹³C]Gly, [U-¹³C]Ala) were purchased from Cambridge Isotope Laboratories Inc., Andover, MA. The synthesis of (AG)₁₅ peptides was performed with standard solid-phase Fmoc chemistry on an Apogee Automated Peptide Synthesizer (AAPPTec, Louisville, KY).⁷ An Fmoc-Gly-PEG-PS resin was used,

and the Fmoc amino acids were coupled with HATU. Peptides were cleaved from the resin by treatment with 90% TFA for 2 h at room temperature. The crude peptide was precipitated and washed repeatedly with cold diethyl ether. The precipitate collected by centrifugation was dried under vacuum and then treated with formic acid to obtain the Silk II form. Confirmation of the Silk II form was obtained from the Ala C β peak pattern in the ¹³C CP/MAS spectrum as reported previously.¹⁵ The peptides synthesized here are summarized in Table 1. Samples (a) and (b) were used for ¹H DQMAS experiments to study the intermolecular arrangement. Samples (c–e) were used for spectral assignments by double CP ¹H–¹³C experiments.

Table 1. Overview of the Isotope-Labeled (AG)₁₅ Samples Prepared Here

- (a) (AG)₁₅
- (b) ([2-d₁]AG)₁₅
- (c) (AG)₇[3-¹³C]AG(AG)₇
- (d) (AG)₇A[U-¹³C]G(AG)₇
- (e) (AG)₇[U-¹³C]A[U-¹³C]G(AG)₇

Solid State DQMAS ¹H NMR and Double CP ¹H–¹³C Correlation NMR. DQMAS (double-quantum magic angle spinning) ¹H NMR and double CP (cross-polarization) ¹H–¹³C correlation NMR experiments were performed at a ¹H resonance frequency of 920 MHz, using a JEOL JNM-ECA920 spectrometer equipped with a ¹H-X double resonance and ultrahighspeed MAS probe at the Institute for Molecular Science (IMS) in Okazaki, Japan.⁹ The sample spinning speed was actively stabilized by a pneumatic solenoid valve such that the spinning fluctuations were less than ± 10 Hz at a spinning rate of 70 kHz. The temperature of the samples increases due to friction under fast MAS and was estimated to be around 333 K at 70 kHz MAS according to Pb(NO₃)₂ temperature calibration. The ¹H rf field strength for the excitation $\pi/2$ pulse (1.29 μ s) was 194 kHz. The ¹H chemical shift was referenced to the peak of silicon rubber and set to 0.12 ppm from TMS. For the ¹H DQMAS measurement, a dipolar homonuclear homogeneous Hamiltonian double-quantum/single-quantum correlation experiment (DH₃DQ-SQ) was employed.³⁸ The 2 τ delay was optimized, giving 0.3 ms for maximum S/N. The DQMAS spectra were obtained every 32 scans at each period in the DQ domain, and the recycle delay was set to 2 s. For ¹H detection in the double CP ¹H–¹³C correlation measurements, the pulse sequence 90^H_y-CP_x-t₁^C-90^C _{ϕ} - τ_d -90^C_y-CP_x-t₂^H was used.³⁹ Here, 90 is a $\pi/2$ pulse, CP is a 4 ms cross-polarization period with a 10% (first) and –10% (second) ramp of ¹³C, t₁ is the evolution period, τ_d is a 5 ms period for dephasing of transverse ¹³C magnetization and ¹H magnetization suppression, and t₂ is the detection period. Superscripts H and C indicate ¹H and ¹³C, and subscripts *x*, *y*, and ϕ indicate rf phases, with $\phi = x$ and *y* for quadrature detection in t₁. The ¹H decoupling amplitude during t₁^C was 27 kHz. The spectrum was obtained after 64 scans at each period in the *y* domain with 512 points.

DARR ¹³C NMR. The ¹³C DARR spectrum (dipolar assisted rotational resonance) of (AG)₇[U-¹³C]A[U-¹³C]G(AG)₇ was obtained after 32 scans at a ¹³C resonance frequency of 400 MHz, using a JEOL ECX400 spectrometer at a spinning speed of 8 kHz with a 4 mm rotor. The $\pi/2$ pulse was 3.8 μ s for ¹³C and 3.4 μ s for ¹H. TPPM ¹H decoupling was performed with a contact time of 2 ms. The mixing time was 500 ms, with a relaxation delay of 2 s. The indirect dimension consisted of 256 data points.

Construction of Two β -Sheet Models with Different Intermolecular Packing Arrangements. The characteristic angles of (ϕ , φ) = (–140°, 140°) for an antiparallel β -sheet structure were used for both Ala and Gly residues in straight (AG)_n chains.¹⁷ To make model 1, starting from the molecular arrangement of the Marsh model¹⁰ viewed along its crystallographic *b*-axis (shown in Figure 1), we rotated strand b (see Figure 2) by 180° around its molecular axis and shifted it along the strand by one residue to change from polar to antipolar structure. Strands a' and b' were generated from a and b

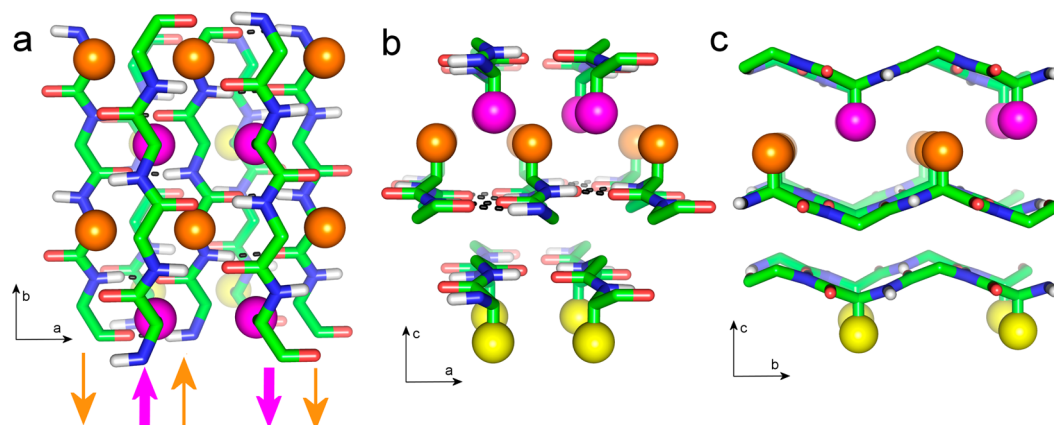


Figure 1. Marsh model of $(AG)_n$. The model is shown from three different orientations, with the relevant unit cell axes shown. Three β -sheet layers are shown. In the top layer, methyl groups are in magenta; in the middle layer they are in orange; and in the bottom layer they are in yellow. Interstrand hydrogen bonds are indicated for the central sheet. The directions of the strands are shown beneath panel (a), with the top strand in magenta and the central strand in orange. This structure corresponds to model (a) of Figure 2.

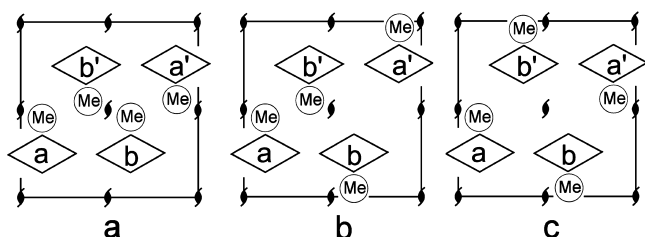


Figure 2. Possible arrangements for the four antiparallel β strands within the unit cell of a $P2_1$ space group, based on the Takahashi model.¹⁴ The strands are shown end-on. Strands a, b and a', b' form antiparallel sheets linked by interstrand hydrogen bonds. An alternating $(Ala-Gly)_n$ structure has all methyl groups on each strand in the same direction, indicated by Me. (a) A polar arrangement, in which all methyl groups in each sheet are pointing in the same direction. The Marsh model¹⁰ has this topology. (b, c) Two alternative antipolar arrangements. The Takahashi models¹⁴ have this arrangement. Form (b) corresponds to model 1 and form (c) to model 2.

using the $P2_1$ operation ($x, y, z \rightarrow -x, y + 1/2, -z$). The strands are aligned along the crystallographic c -axis. To make model 2, strands a and b (Figure 2) were rotated by 90° around the a -axis. Then the b -axis was redefined to be aligned along the molecular axis. The upper two molecules were generated from the lower two using the $P2_1$ operation. In order to avoid steric clash between strands a, b and strands a', b', strands a and b were shifted along their axis by half a residue. Both models were then energy minimized using the pcff force field of Discover (Accelrys Inc., San Diego, CA), using the cell dimensions reported by Takahashi et al.:¹⁴ $a = 9.38 \text{ \AA}$, $b = 9.49 \text{ \AA}$, $c = 6.98 \text{ \AA}$, and space group $P2_1$.

As a final step, geometry optimization was carried out under periodic boundary conditions using the CASTEP program (Accelrys Inc., San Diego, CA).¹⁹ We used the generalized gradient approximation (GGA) for the exchange correlation energy based on the Perdew, Bruke, and Ernzerhof (PBE) functional and ultrasoft pseudopotentials with a plane-wave energy cutoff of 380 eV. A $5 \times 2 \times 3$ Monkhorst–Pack k -point grid was used for Brillouin zone sampling.

^1H , ^{13}C , and ^{15}N NMR Chemical Shift Calculations. The chemical shifts of ^1H , ^{13}C , and ^{15}N in the two antiparallel β -sheet structures with different intermolecular arrangements were calculated using the GIPAW method.²³ The PBE approximation and “on the fly” pseudopotentials were used. The energy cutoff of the plane wave was set to 610 eV, and a $5 \times 2 \times 3$ Monkhorst–Pack k -point grid was used as described above. The chemical shift reference of the calculated chemical shifts was determined by minimizing the difference between the observed and calculated chemical shifts without changing the

relative chemical shift differences between the peaks.¹⁹ The reference values were 30.51, 171.31, and 197.22 ppm for the ^1H , ^{13}C , and ^{15}N nuclei, respectively. All calculations were carried out using the NMR-CASTEP program.

RESULTS AND DISCUSSION

DQMAS ^1H NMR Spectrum of $(AG)_{15}$ in the Silk II Form. By combining the use of a microcoil probe head with an

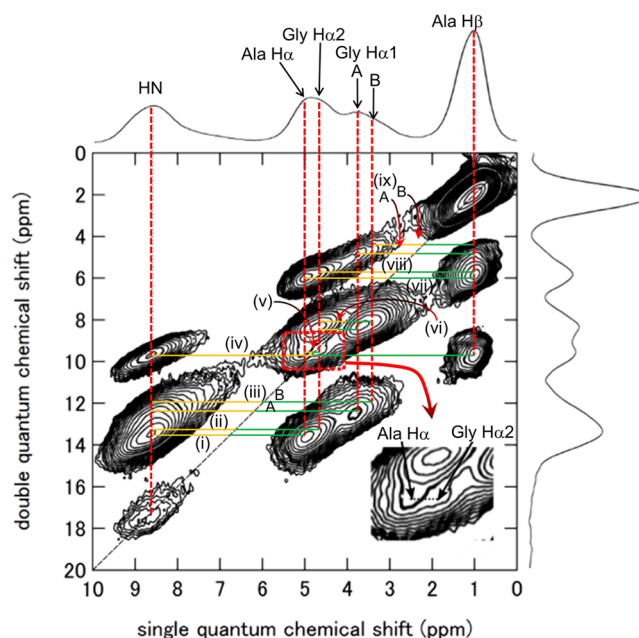


Figure 3. ^1H DQMAS spectrum of $(AG)_{15}$ in the Silk II form: (i) $\text{AlaH}\alpha\text{-AlaHN}$, (ii) $\text{GlyH}\alpha2\text{-GlyHN}$, (iii) $\text{GlyH}\alpha1\text{-GlyHN}$, (iv) $\text{AlaH}\beta\text{-AlaHN}$, (v) $\text{AlaH}\alpha\text{-GlyH}\alpha2$, (vi) $\text{GlyH}\alpha2\text{-GlyH}\alpha1$, (vii) $\text{AlaH}\alpha\text{-AlaH}\beta$, (viii) $\text{GlyH}\alpha2\text{-AlaH}\beta$, and (ix) $\text{GlyH}\alpha1\text{-AlaH}\beta$.

ultrahigh-field NMR spectrometer at 920 MHz, we obtained a well-resolved solid state ^1H NMR spectrum of $(AG)_{15}$ in the Silk II form. The ^1H chemical shifts were assigned using a DQMAS ^1H NMR experiment, as illustrated in Figure 3. From high field to low field, the peaks are assigned as $\text{AlaH}\beta$, $\text{GlyH}\alpha1$ (upfield), $\text{GlyH}\alpha2$ (downfield), $\text{AlaH}\alpha$, and H_N (both Ala and Gly). Thus, for glycine the two $\text{H}\alpha$ protons are observed

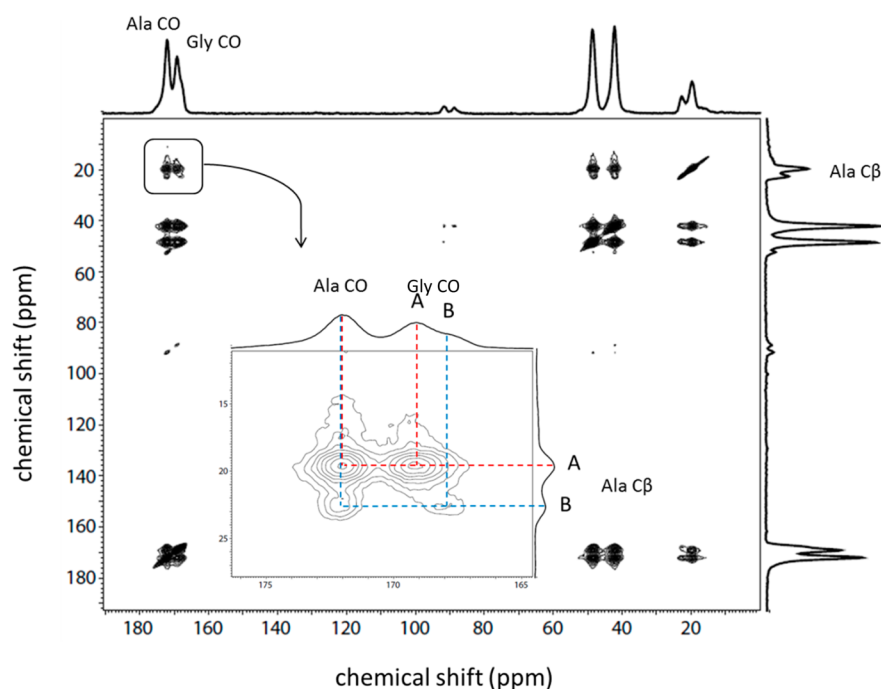


Figure 4. ^{13}C – ^{13}C DARR spectrum of $(\text{AG})_7[\text{U-}^{13}\text{C}]\text{A}[\text{U-}^{13}\text{C}]\text{G}(\text{AG})_7$ in the Silk II form. The inset shows the correlation between the CO and Ala $\text{C}\beta$ region.

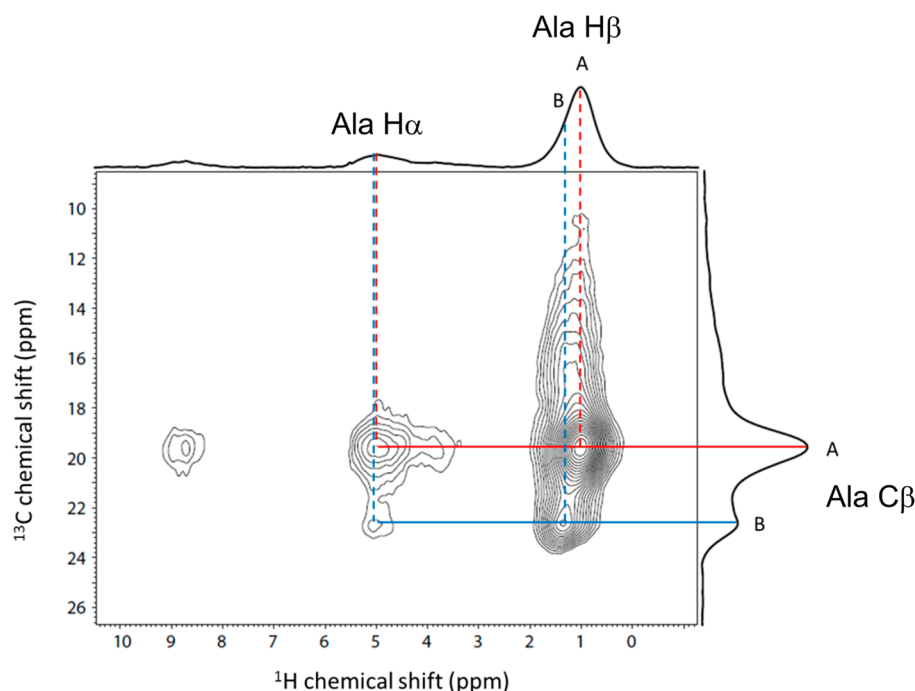


Figure 5. Double CP ^1H – ^{13}C spectrum of $(\text{AG})_7[3\text{-}^{13}\text{C}]\text{AG}(\text{AG})_7$ in the Silk II form, showing the correlations of Ala $\text{C}\beta$ with Ala $\text{H}\beta$ and $\text{H}\alpha$.

separately and with a large chemical shift difference. This discrimination is generally feasible in the solid state, given the lack of motions around the backbone chains in silk fibroin. A more detailed assignment is performed below with the help of specifically isotope-labeled peptides, and the relative ^1H – ^1H distances are measured and discussed in the last section.

Determination of the ^1H and ^{13}C Chemical Shifts in the Heterogeneous Domains. The ^{13}C – ^{13}C DARR spectrum of $(\text{AG})_7[\text{U-}^{13}\text{C}]\text{A}[\text{U-}^{13}\text{C}]\text{G}(\text{AG})_7$ was obtained as shown in Figure 4. In agreement with our previous results,^{15,16}

we see two well-resolved Ala $\text{C}\beta$ peaks in an intensity ratio of approximately 2:1, which are named A and B, respectively, representing the two packing arrangements. From the correlations between these two Ala $\text{C}\beta$ peaks and the Gly CO region, and based on the relative peak intensities, two peaks within the Gly CO signal could also be assigned as the A and B components. Within the Ala CO peak, on the other hand, there were no chemical shift differences resolved. Further assignment was obtained for the solid state NMR ^1H spectrum of $(\text{AG})_{15}$. A ^1H – ^{13}C double CP spectrum³⁹ of $(\text{AG})_7[3\text{-}^{13}\text{C}]$ -

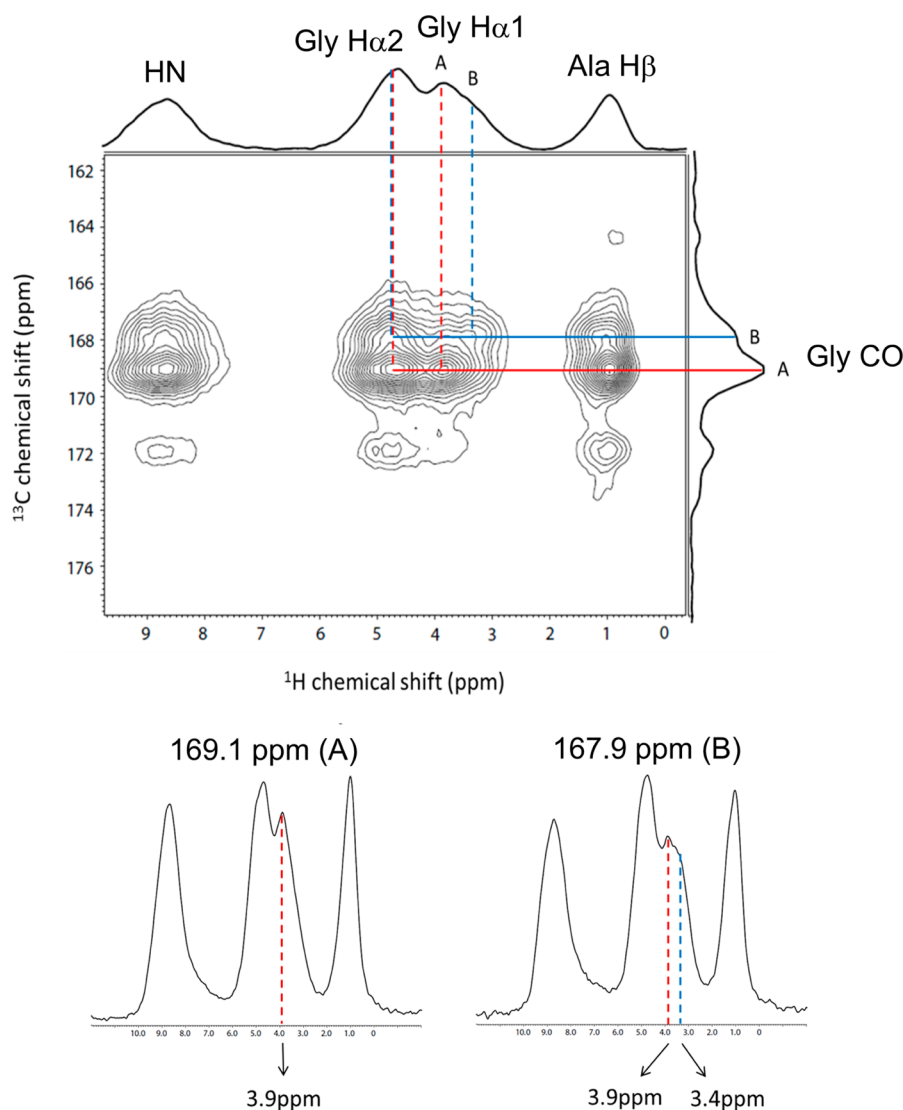


Figure 6. ^1H – ^{13}C double CP spectrum (upper) and of $(\text{AG})_7\text{A}[\text{U-}^{13}\text{C}]\text{G}(\text{AG})_7$ in the Silk II form. The 1D ^1H spectra (lower) show the relevant slices at 167.9 and 169.1 ppm corresponding to the two components A and B within the Gly CO region.

Table 2. ^1H , ^{13}C , and ^{15}N Chemical Shifts Calculated and Observed for $(\text{AG})_{15}$ in the Silk II Form^a

^1H		Gly HN	Ala HN	Ala H α	Gly H α 2	Gly H α 1	Ala H β
A	calc	9.6	9.3	5.0	4.6	3.1	0.1
	obs	8.7	8.7	5.0	4.6	3.9	1.0
B	calc	9.2	9.3	5.6	4.8	2.6	0.6
	obs	8.7	8.7	5.0	4.6	3.4	1.3
^{13}C		Ala CO	Gly CO	Ala C α	Gly C α	Ala C β	
A	calc	175.6	171.4	48.8	41.1	16.3	
	obs	172.6	169.1	49.2	43.0	19.6	
B	calc	176.1	170.1	48.0	42.1	21.8	
	obs	172.6	167.9	49.0	43.0	22.4	
^{15}N		Ala N			Gly N		
A	calc	97.0			84.3		
	obs	98.0			86.0		
B	calc	104.9			80.9		
	obs	101.0			82.0		

^aCalculated shifts are tabulated assuming that model 1 corresponds to A and model 2 to B.

$\text{AG}(\text{AG})_7$ in the Silk II form was acquired as shown in Figure 5. The chemical shifts of the A and B components within the Ala H β and H α peaks were determined from their correlation with the two well-resolved Ala C β signals. A small chemical shift difference of 0.3 ppm was clearly discernible in the Ala H β peak. Within the Ala H α region, on the other hand, chemical shift differences were not resolved. Similarly, we used the ^1H – ^{13}C double CP spectrum of $(\text{AG})_7\text{A}[\text{U-}^{13}\text{C}]\text{G}(\text{AG})_7$ in Figure 6 to assign the two components A (3.9 ppm) and B (3.4 ppm) within the Gly H α 1 signal, while any chemical shift differences in the Gly H α 2 region could not be resolved. The observed chemical shift data are summarized in Table 2.

Construction of Two Antiparallel β -Sheet Structures with Different Intermolecular Packing Arrangements. It has been previously reported^{15,16} that the ^{13}C CP/MAS NMR spectra of both the model peptide $(\text{AG})_{15}$ as well as the natural Cp-fraction of *B. mori* silk fibroin in the Silk II form show a multicomponent Ala methyl peak. This Ala C β peak was resolved and assigned to three components, namely two different kinds of β -sheet structure (19.2 and 22.3 ppm), plus a distorted β -sheet and/or random coil conformation (16.1 ppm), the latter presumably originating from loops and turns at

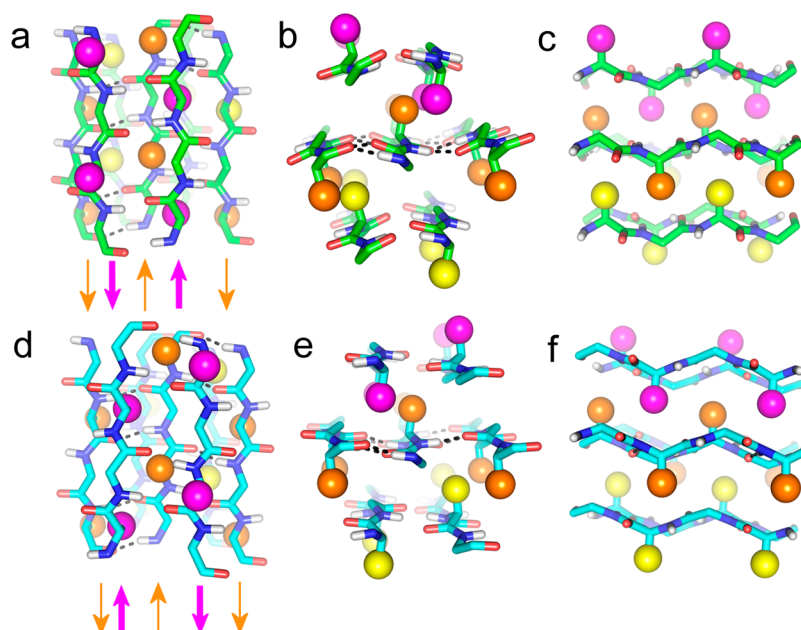


Figure 7. Model 1 (top row) and model 2 (bottom row), shown from three orthogonal orientations. The same color scheme is used as for Figure 1. Model 1 corresponds to structure (b) in Figure 2 and model 2 to structure (c). In model 1, the molecular axis is along the crystallographic axis *c*, and in model 2, the molecular axis is along the crystallographic axis *b*.

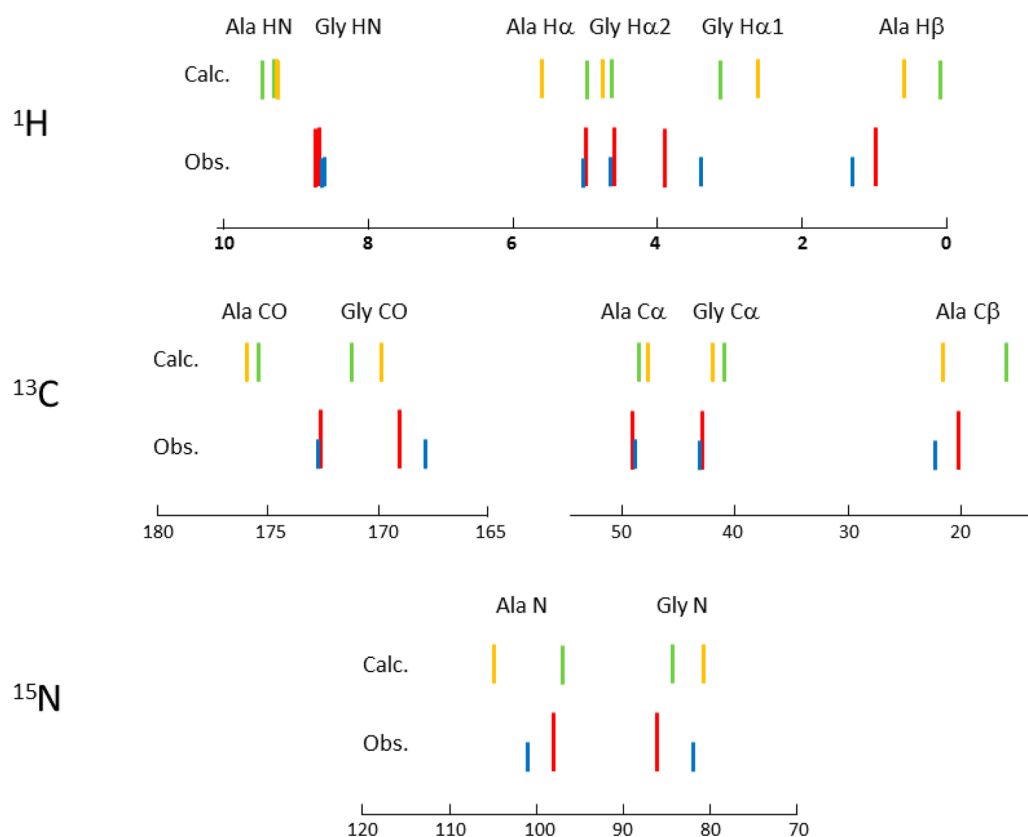


Figure 8. Stick spectra of the calculated and observed ^1H , ^{13}C , and ^{15}N chemical shifts (in ppm) for $(\text{AG})_{15}$ in the intrinsically heterogeneous Silk II form. The observed shifts are colored red and blue to correspond to the set of peaks A and B, respectively, which are in an intensity ratio of approximately 2:1. The calculated shifts are colored green and orange for models 1 and 2, respectively.

each end of the antiparallel crystalline regions. However, there has been no further discussion so far about the meaning of the first two peaks assigned to the two types of antiparallel β -sheet structures. The large chemical shift difference of about 3 ppm

within the Ala $\text{C}\beta$ peak cannot be interpreted in terms of different torsion angles for the Ala residue in the β -sheet region.⁴⁰ Therefore, the chemical shift difference must be attributed to differences in the intermolecular packing of the β -

Table 3. Closest ^1H – ^1H Distances of Protons Evaluated for the Two Different Models of the Silk II Structure^a

	I		II		I		II		III	
Marsh model	Gly H α 2	Gly H α 1	Gly H α 2	Gly H α 1	Ala H α	Ala H β	Ala H α	Ala H β	Ala H α	Ala H β
Gly H α 2	<u>1.99</u>	<u>3.43</u>	4.30	<u>3.75</u>	5.90	5.65	4.12	<u>3.62</u>	4.52	4.60
Gly H α 1	<u>3.43</u>	4.38	<u>3.75</u>	4.05	5.31	6.59	4.16	<u>4.50</u>	4.37	5.19
model proposed	I		II		I		II		III	
	Gly H α 2	Gly H α 1	Gly H α 2	Gly H α 1	Ala H α	Ala H β	Ala H α	Ala H β	Ala H α	Ala H β
1 Gly H α 2	5.67	5.02	4.61	4.05	<u>2.43</u>	<u>3.71</u>	4.86	<u>3.36</u>	4.49	4.59
Gly H α 1	5.02	6.55	4.05	4.37	4.04	<u>3.29</u>	<u>3.63</u>	<u>2.81</u>	4.31	5.20
2 Gly H α 2	5.57	5.29	4.83	<u>3.50</u>	<u>2.23</u>	<u>3.21</u>	4.86	<u>2.90</u>	4.46	4.56
Gly H α 1	5.29	6.84	<u>3.50</u>	4.57	<u>3.73</u>	<u>3.76</u>	<u>3.10</u>	<u>3.00</u>	4.45	5.30

^aI: two ^1H nuclei in different strands that are located within the same β -sheet plane. II: two ^1H nuclei in different strands that are located in neighboring β -sheet planes. III: two ^1H nuclei within the same strand. The underlined numbers indicate distances of less than 4 Å.

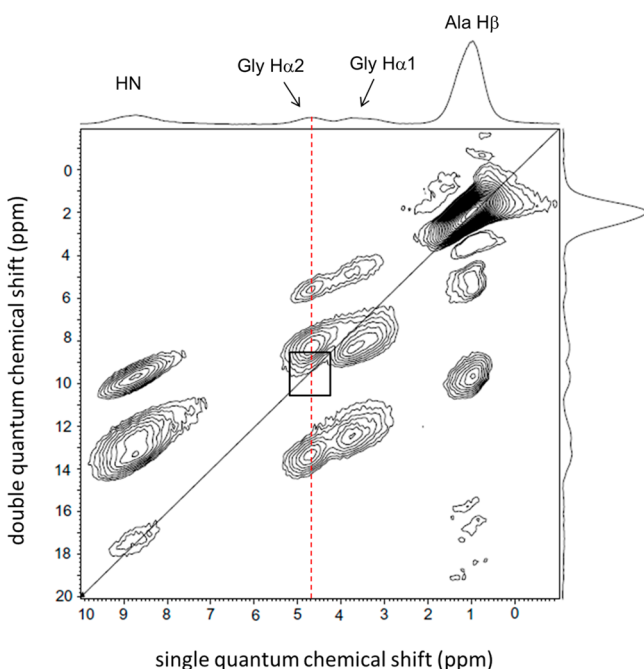


Figure 9. ^1H DQMAS spectrum of deuterium-labeled $([2\text{-d}_1]\text{AG})_{15}$ in the Silk II form to remove potential overlap in the H α region (cf. Figure 3). It is clear that there are no Gly H α –Gly H α peaks on the diagonal.

strands. In the Marsh model, all molecules are in identical environments. It is therefore not readily reconciled with the experimental data. We have previously tried to interpret these two peaks using the Takahashi model, which has two different packing arrangements within the crystal, occupied statistically in the ratio 2:1, and is therefore in much better agreement with the NMR data.^{15,16} However, the Takahashi model is clearly not correct in detail. In particular, the interstrand $\text{NH}\cdots\text{OC}$ hydrogen bond lengths are 2.1 Å for Ala and 2.6 Å for Gly, whereas the experimentally observed Ala and Gly H_N chemical shifts are both 8.7 ppm,²¹ implying hydrogen bond lengths of around 1.8 Å for both Ala and Gly.⁴¹ We therefore explored alternative models based on the Takahashi model, but with better geometry.

Takahashi et al.¹⁴ note that an antiparallel β -sheet composed of alternating Gly and Ala can be constructed in two ways: a *polar* arrangement in which the backbone hydrogen bonds are Ala \cdots Ala and Gly \cdots Gly, and the methyl groups in one sheet are all pointing in the same direction; or an *anti-polar* arrangement

in which the backbone hydrogen bonds are Ala \cdots Gly, and the methyl groups in a sheet alternate, pointing up in one strand and down in the next (Figure 2). They concluded that the crystallographic data fit an antipolar model better. By contrast, the Marsh model (Figure 1) is polar, which forces sheets to be alternately close and distant. We therefore constructed models with antipolar sheets.

Previously,¹⁷ we determined the torsion angles in the *B. mori* silk fibroin fiber from solid state NMR orientational constraints to be $(-140^\circ, 142^\circ)$ for Ala and $(-139^\circ, 135^\circ)$ for Gly, within an experimental error of $\pm 5^\circ$. We thus used the typical β -sheet torsion angles of $(-140^\circ, 140^\circ)$ for both the Ala and Gly residues to generate model structures of $(\text{AG})_{15}$. We also used the unit cell dimensions of the *B. mori* silk fibroin fiber as reported by Takahashi et al.¹⁴ Given these constraints, the problem is limited to how one sheet packs on top of its neighbor. Any stereochemically viable model must have the strands in one sheet displaced by roughly half an interstrand spacing compared to its neighbor (Figure 2b,c).

On this basis, we constructed and refined two structural models with different intermolecular packing of the β -strands in the unit cell: model 1 and model 2 (Figure 7). Model 1 was consistently of slightly lower energy than model 2. Figure 7 shows both models with the central sheet in the same orientation to emphasize the difference in packing of the top sheet against the middle one. A key difference is that the Ala methyls are positioned differently. Model 1 has the packing shown in Figure 2b. The methyls of the top sheet that point down to the central sheet point roughly toward the Gly H α , in the spaces between the pairs of interstrand Gly \cdots Ala hydrogen bonds. By contrast, in model 2 (corresponding to Figure 2c), the methyls point to the center of the pair of interstrand Gly \cdots Ala hydrogen bonds and are thus shifted along the strand by one residue. We note that because both models were energy minimized against the crystal dimensions of Takahashi et al.,¹⁴ they are both consistent with the crystallographic data.

^1H , ^{13}C , and ^{15}N Chemical Shift Calculation of Model $(\text{AG})_{15}$ Structures. ^1H , ^{13}C , and ^{15}N chemical shifts were calculated for models 1 and 2 using GIPAW and are summarized in Table 2. The output files after CASTEP calculations are listed in the Supporting Information: Tables 1S (model 1 = A) and 2S (model = B). Figure 8 shows the corresponding stick spectra for the calculated and observed chemical shifts, from which it can be seen that the calculated shifts for model 1 fit the positions of experimental peaks A well, and calculated model 2 shifts fit experimental peaks B well, while the alternative assignment (model 1 = B and model 2 =

A) fits poorly. In particular, the covariance⁴² for 1 = A and 2 = B is 0.23 ppm², while for 1 = B and 2 = A it is 0.57 ppm², clearly indicating that the correct assignment is 1 = A and 2 = B. This pairing is in agreement with the calculated lower energy for model 1. We therefore equate model 1 with peaks A and model 2 with peaks B. The agreement between calculated and observed ¹H shifts is reasonable. The ¹H chemical shift calculation of model 1 makes it possible now to assign the two Gly H α peaks. Namely, the H α of the Gly residue observed at lower field at 4.6 ppm can be assigned to the H α located in the β -sheet plane. This feature is important when we come to discuss the β -sheet assembly in the light of the DQMAS ¹H NMR data, where the Ala methyl signal corresponding to model 1 was obtained at higher field than for model 2.

For the ¹³C chemical shifts, the agreement between the observed and calculated chemical shifts is excellent, given that the entire chemical shift range from the highest field Ala C β to the lowest field Ala CO peak could be well reproduced, and the chemical shift differences between the different carbons also agree very well. In addition, the peak of Ala C β was correctly found to appear at a higher field in model 1 than in model 2. The experimental finding that components A and B were not resolved in the ¹³C signals of Gly C α , Ala C α , and Ala CO is also in agreement with the small calculated chemical shift differences between models 1 and 2.

Finally, the calculated and previously observed ¹⁵N chemical shifts⁴³ are compared for the two models. In this case the two peaks of Ala and Gly were well resolved, so their relative peak positions as well as the chemical shift difference could be compared. The agreement is also excellent, and the two peaks corresponding to models 1 and 2 could be assigned for both ¹⁵N nuclei. The goodness of fit for ¹³C and ¹H can be compared to literature values. Using the assignment of model 1 = A and model 2 = B, the root-mean-square difference between calculated and observed shifts is 2.2 ppm for ¹³C and 0.6 ppm for ¹H (or 0.4 ppm omitting amide protons, for which chemical shift calculations are particularly difficult because of their great sensitivity to hydrogen bonding). This can be compared to other comparisons between GIPAW calculations and experimental solid-state shifts for small organic compounds: 2.5 ppm for ¹³C and 0.3 ppm for ¹H (penicillin G);⁴⁴ 3.4 ppm for ¹³C (testosterone);²⁵ an average of 3.1 ppm for ¹³C and 0.3 ppm for ¹H (thymol).⁴⁵ Thus, the chemical shift calculation overall reproduces the observed chemical shifts very well for all three nuclei, giving us confidence in the accuracy of the models. We therefore propose that *B. mori* (Ala-Gly)_n silk II consists of antipolar antiparallel sheets arranged statistically in the arrangements shown in models 1 and 2, with a preference of about 2:1 for model 1 vs model 2.

Validation of the New Heterogeneous Model from DQMAS ¹H NMR. A further test for the validity of the models derived here comes from ¹H–¹H distances observed in DQMAS ¹H NMR spectra, which typically must be within about 4 Å to give rise to observable cross-peaks.¹⁹ A set of nine ¹H–¹H correlation signals is indicated in Figure 3. We examined the ¹H–¹H distances underlying these observed ¹H–¹H correlations by inspecting the list of ¹H–¹H distances calculated from our models, and comparing them to the Marsh model. Particularly diagnostic are the ¹H–¹H distances in which either Gly H α 1 or GlyH α 2 protons are involved, which are listed in Table 3. All distances calculated to be less than 4 Å in one or both models (underlined in Table 3) are present in

the spectrum, as expected. By contrast, several distances that are very short in the Marsh model do not give rise to observable peaks in the spectrum, providing strong evidence that the Marsh model does not correspond with the experimental data:

A given contact for GlyH α 1–GlyH α 1 or GlyH α 2–GlyH α 2 indicates a distance between two ¹H nuclei that are located in different strands.

(1) Cross-peak v is between Gly H α 2 and Ala H α . This distance is very short in both models, but is longer than 4 Å in the Marsh model.

(2) Cross-peaks viii and ix are from Ala H β to Gly H α 1 and H α 2. Both these distances are short in models 1 and 2. However, in the Marsh model these distances are both well over 4 Å.

(3) In the Marsh model, the Gly H α 2 protons in adjacent β -strands are very close to one another, so a diagonal peak for Gly H α 2 should be detected. This feature, however, is difficult to judge from Figure 1 because the Gly H α 2 and Ala H α peaks overlap in the relevant spectral region. We therefore synthesized deuterium-labeled ([2-d]AG)₁₅ and acquired another DQMAS ¹H NMR spectrum. As seen in Figure 9, there is clearly no Gly H α 2 peak on the diagonal, now that the Ala H α signal at around 5.0 ppm has been removed. This observation provides very strong evidence that polar models, such as in the Marsh model, cannot be correct.

In summary, we have shown that *B. mori* (Ala-Gly)_n silk II exists in two packing arrangements A and B in a ratio of approximately 2:1. We have presented two models (1 and 2, corresponding respectively to A and B), which fit all experimental data, in particular crystallographic, chemical shifts and ¹H–¹H dipolar contacts. We have demonstrated that silk II must be an antipolar, not a polar, packing. We propose that crystalline Silk II is a statistical mixture of these two packing arrangements, in a ratio 2:1. (The coordinates of the new Silk II model are listed in the Supporting Information: Table 1S (model 1 = A) and 2S (model = B).)

■ ASSOCIATED CONTENT

● Supporting Information

Coordinates of the new Silk II model are listed in Table 1S (model 1 = A) and 2S (model = B). This material is available free of charge via the Internet at <http://pubs.acs.org>.

■ AUTHOR INFORMATION

Corresponding Author

*E-mail: (T.A.) asakura@cc.tuat.ac.jp.

Notes

The authors declare no competing financial interest.

■ ACKNOWLEDGMENTS

T.A. acknowledges support by a Grant-in-Aid for Scientific Research from the Ministry of Education, Science, Culture and Supports of Japan (23245045, 25620169, 26248050) and the Ministry of Agriculture, Forestry and Fisheries of Japan (Agri-Health Translational Research Project). Computation time was provided by the SuperComputer System, Institute for Chemical Research, Kyoto University.

■ REFERENCES

- (1) Fu, C.; Shao, Z.; Vollrath, F. *Chem. Commun.* **2009**, 43, 6515–6529.
- (2) Brown, J.; Lu, C. L.; Coburn, J.; Kaplan, D. L. *Acta Biomater.* **2014**, 10, 776–784.

- (3) Tokareva, O.; Jacobsen, M.; Buehler, M.; Wong, J.; Kaplan, D. L. *Acta Biomater.* **2013**, *6*, 651–663.
- (4) Lin, Y.; Xia, X.; Shang, K.; Elia, R.; Huang, W.; Cebe, P.; Leisk, G.; Omenetto, F.; Kaplan, D. L. *Biomacromolecules* **2013**, *14*, 2629–2635.
- (5) Boulet-Audet, M.; Terry, A. E.; Vollrath, F.; Holland, C. *Acta Biomater.* **2014**, *10*, 776–784.
- (6) Asakura, T.; Suzuki, Y.; Nakazawa, Y.; Yazawa, K.; Holland, G. P.; Yarger, J. L. *Prog. Nucl. Magn. Reson. Spectrosc.* **2013**, *69*, 23–68.
- (7) Asakura, T.; Ashida, J.; Yamane, T.; Kameda, T.; Nakazawa, Y.; Ohgo, K.; Komatsu, K. *J. Mol. Biol.* **2001**, *306*, 291–305.
- (8) Asakura, T.; Ohgo, K.; Komatsu, K.; Kanenari, M.; Okuyama, K. *Macromolecules* **2005**, *38*, 7397–7403.
- (9) Asakura, T.; Suzuki, Y.; Yazawa, K.; Aoki, A.; Nishiyama, Y.; Nishimura, K.; Suzuki, F.; Kaji, H. *Macromolecules* **2013**, *46*, 8046–8050.
- (10) Marsh, R. E.; Corey, R. B.; Pauling, L. *Biochim. Biophys. Acta* **1955**, *16*, 1–34.
- (11) Fraser, B.; MacRae, T. P. *Conformations of Fibrous Proteins and Related Synthetic Polypeptides*; Academic Press: New York, 1973.
- (12) Lotz, B.; Cesari, F. C. *Biochimie* **1979**, *61*, 205–214.
- (13) Fossey, S. A.; Nemethy, G.; Gibson, K. D.; Scheraga, H. A. *Biopolymers* **1991**, *31*, 1529–1541.
- (14) Takahashi, Y.; Gehoh, M.; Yuzuriha, K. *Int. J. Biol. Macromol.* **1999**, *24*, 127–138.
- (15) Asakura, T.; Yao, J.; Yamane, T.; Umemura, K.; Ulrich, A. S. *J. Am. Chem. Soc.* **2002**, *124*, 8794–8795.
- (16) Asakura, T.; Yao, J. *Protein Sci.* **2002**, *11*, 2706–2713.
- (17) Demura, M.; Minami, M.; Asakura, T.; Cross, T. A. *J. Am. Chem. Soc.* **1998**, *120*, 1300–1308.
- (18) Schnell, I.; Brown, S. P.; Low, H. Y.; Ishida, H.; Spiess, H. W. *J. Am. Chem. Soc.* **1998**, *120*, 11784–11795.
- (19) Brown, S. P. *Solid State Nucl. Magn. Reson.* **2012**, *41*, 1–27 and references therein.
- (20) Yamauchi, K.; Yamasaki, S.; Takahashi, R.; Asakura, T. *Solid State Nucl. Magn. Reson.* **2010**, *38*, 27–30.
- (21) Yazawa, K.; Suzuki, F.; Nishiyama, Y.; Ohata, T.; Aoki, A.; Nishimura, K.; Kaji, H.; Shimizu, T.; Asakura, T. *Chem. Commun.* **2012**, *48*, 11199–11201.
- (22) Asakura, T.; Yazawa, K.; Horiguchi, K.; Suzuki, F.; Nishiyama, Y.; Nishimura, K.; Kaji, H. *Biopolymers* **2013**, *101*, 13–20.
- (23) Pickard, C. J.; Mauri, F. *Phys. Rev. B* **2001**, *63*, 245101.
- (24) Gervais, C.; Profeta, M.; Lafond, V.; Bonhomme, C.; Azais, T.; Mutin, H.; Pickard, C. J.; Mauri, F.; Babonneau, F. *Magn. Reson. Chem.* **2004**, *42*, 445–452.
- (25) Harris, R. K.; Joyce, S. A.; Pickard, C. J.; Cadars, S.; Emsley, L. *Phys. Chem. Chem. Phys.* **2006**, *8*, 137–143.
- (26) Harris, R. K.; Hodgkinson, P.; Pickard, C. J.; Yates, J. R.; Zorin, V. *Magn. Reson. Chem.* **2007**, *45*, S174–S186.
- (27) Shao, L. M.; Yates, J. R.; Titman, J. J. *J. Phys. Chem. A* **2007**, *111*, 13126–13132.
- (28) Pickard, C. J.; Salager, E.; Pintacuda, G.; Elena, B.; Emsley, L. *J. Am. Chem. Soc.* **2007**, *129*, 8932–8933.
- (29) Uldry, A. C.; Griffin, J. M.; Yates, J. R.; Perez-Torralba, M.; Maria, M. D. S.; Webber, A. L.; Beaumont, M. L. L.; Samoson, A.; Claramunt, R. M.; Pickard, C. J.; Brown, S. P. *J. Am. Chem. Soc.* **2008**, *130*, 945–954.
- (30) Cadars, S.; Lesage, A.; Pickard, C. J.; Sautet, P.; Emsley, L. *J. Phys. Chem. A* **2009**, *113*, 902–911.
- (31) *NMR Crystallography*; Harris, R. K., Wasylishen, R. E., Duer, M., Eds.; Wiley: Chichester, 2009.
- (32) Salager, E.; Day, G. M.; Stein, R. S.; Pickard, C. J.; Elena, B.; Emsley, L. *J. Am. Chem. Soc.* **2010**, *132*, 2564–2566.
- (33) Johnston, J. C.; Iulicci, R. J.; Facelli, J. C.; Fitzgerald, G.; Mueller, K. T. *J. Chem. Phys.* **2009**, *131*, 144503.
- (34) Suzuki, F.; Fukushima, T.; Fukuchi, M.; Kaji, H. *J. Phys. Chem. C* **2013**, *117*, 18809–18817.
- (35) Asakura, T.; Demura, M.; Date, T.; Miyashita, N.; Ogawa, K.; Williamson, M. P. *Biopolymers* **1997**, *41*, 193–203.
- (36) Asakura, T.; Sugino, R.; Yao, J.; Takashima, H.; Kishore, R. *Biochemistry* **2002**, *41*, 4415–4424.
- (37) Yao, J.; Ohgo, K.; Sugino, R.; Kishore, R.; Asakura, T. *Biomacromolecules* **2004**, *5*, 1763–1769.
- (38) Deschamps, M.; Fayon, F.; Cadars, S.; Rollet, A.; Massiot, D. *Phys. Chem. Chem. Phys.* **2011**, *13*, 8024–8030.
- (39) Ishii, Y.; Yesinowski, J. P.; Tycko, R. *J. Am. Chem. Soc.* **2001**, *123*, 2921–2922.
- (40) Asakura, T.; Iwadate, M.; Demura, M.; Williamson, M. P. *Int. J. Biol. Macromol.* **1999**, *24*, 167–171.
- (41) Asakura, T.; Taoka, K.; Demura, M.; Williamson, M. P. *J. Biomol. NMR* **1995**, *6*, 227–236.
- (42) Czernek, J.; Brus, J. *Chem. Phys. Lett.* **2014**, *608*, 334–339.
- (43) Suzuki, Y.; Takahashi, R.; Shimizu, T.; Tansho, M.; Yamauchi, K.; Williamson, M. P.; Asakura, T. *J. Phys. Chem. B* **2009**, *113*, 9756–9761.
- (44) Mifsud, N.; Elena, B.; Pickard, C. J.; Lesage, A.; Emsley, L. *Phys. Chem. Chem. Phys.* **2006**, *8*, 3418–3422.
- (45) Salager, E.; Stein, R. S.; Packard, C. J.; Elena, B.; Emsley, L. *Phys. Chem. Chem. Phys.* **2009**, *11*, 2610–2621.